Title

Inward-to-outward assembly of amine-functionalized carbon dots and polydopamine to Shewanella oneidensis MR-1 for high-efficiency, microbial-photoreduction of Cr(VI)

Journal

Chemosphere, 307(Pt 3)

ISSN

0045-6535

Authors

Li, Jian
Wang, Feng
Zhang, Jing
et al.

Publication Date

2022-11-01

DOI

10.1016/j.chemosphere.2022.135980

Peer reviewed

Chemosphere 307 (2022) 135980

Contents lists available at ScienceDirect

Chemosphere

journal homepage: www.elsevier.com/locate/chemosphere

Inward-to-outward assembly of amine-functionalized carbon dots and polydopamine to *Shewanella oneidensis* MR-1 for high-efficiency, microbial-photoreduction of Cr(VI)

Jian Li [a,1], Feng Wang [a,1], Jing Zhang [d], Honghui Wang [d], Chongyuan Zhao [a], Lielin Shu [a], Peng Huang [a], Yejing Xu [a], Zhiying Yan [c], Randy A. Dahlgren [a,b], Zheng Chen [a,d,*]

[a] School of Public Health & Management, Wenzhou Medical University, Wenzhou, 325035, People's Republic of China
[b] Department of Land, Air & Water Resources, University of California, Davis, CA, 95616, USA
[c] CAS Key Laboratory of Environmental & Applied Microbiology, Environmental Microbiology Key Laboratory of Sichuan Province, Chengdu Institute of Biology, Chinese Academy of Sciences, Chengdu, 610041, People's Republic of China
[d] School of Environmental Science & Engineering, Tan Kah Kee College, Xiamen University, Zhangzhou, 363105, People's Republic of China

HIGHLIGHTS

- A novel photosensitized biohybrid was fabricated using inward-to-outward assembly of NCDs and PDA to S. oneidensis MR-1.
- Biohybrids enhance the bulk electron flux by harvesting reducing equivalents and photoelectrons and reducing powers.
- Increased interfacial conductivity ensures rapid intracellular/extracellular charge transport in biohybrids.
- Biohybrids withstand high Cr(VI) exposure and achieve highly efficient microbial-photoreduction of Cr(VI).

GRAPHICAL ABSTRACT

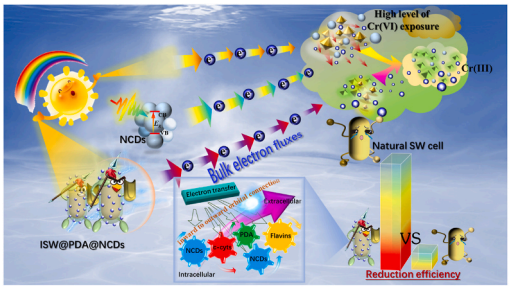

ARTICLE INFO

Handling Editor: CHANG MIN PARK

Keywords:
Shewanella
Amine-functionalized carbon dots
Hexavalent chromium
Photoelectrons
Biohybrid

ABSTRACT

A novel photosensitized living biohybrid was fabricated by inward-to-outward assembly of amine-functionalized carbon dots (NCDs) and polydopamine (PDA) to *Shewanella oneidensis* MR-1 and applied for high-efficiency, microbial-photoreduction of Cr(VI). Within a 72 h test period, biohybrids achieved a pronounced catalytic reduction capacity (100%) for 100 mg/L Cr(VI) under visible illumination, greatly surpassing the poor capacity (only 2.5%) displayed by the wild strain under dark conditions. Modular configurations of NCDs and PDA afforded biohybrids with a large electron flux by harvesting extracellular photoelectrons generated from illuminated NCDs and increasing reducing equivalents released from an enlarged intracellular NADH/NAD^+ pool. Further, increased production of intracellular c-type cytochromes and extracellular flavins resulting from the modular configuration enhanced the biohybrid electron transport ability. The enhancement of electron transport was also attributed to more conductive conduits at NCDs-PDA junction interfaces. Moreover, because NCDs are highly reductive, the enhanced Cr(VI) reduction was also attributed to direct reduction by the NCDs and the direct Cr(VI) reduction by sterile NCDs-assembled biohybrid was up to 20% in the dark. Overall, a highly

* Corresponding author. School of Public Health and Management, Wenzhou Medical University, Wenzhou, 325035, People's Republic of China.
E-mail address: chenzheng_new@163.com (Z. Chen).
[1] These authors were considered as the co-first authors.

https://doi.org/10.1016/j.chemosphere.2022.135980
Received 29 June 2022; Received in revised form 27 July 2022; Accepted 5 August 2022
Available online 10 August 2022

efficient strategy for removal/transformation of Cr(VI) by using NCD-assembled photosensitized biohybrids was proposed in this work, which greatly exceeded the performance of Cr(VI)-remediation strategies based on conventional microbial technologies.

1. Introduction

Microbial transformation of Cr(VI) is purported to be an effective, economical and technologically feasible biotechnology for removal of Cr (VI) from wastewater, whereby highly toxic Cr(VI) is reduced to insoluble and less toxic Cr(III)-bearing precipitates (Verma et al., 2015; Khare et al., 2016). *Shewanella* is a representative electrically active bacteria (EAB) capable of reducing Cr(VI) through an extracellular electron transfer (EET) pathway (Li et al., 2019; Luo et al., 2019). However, inherent inefficient EET abilities and a fragile biological tolerance of most natural EABs limit their practical applications. These limitations result in an insufficient electron flux for efficient Cr(VI) reduction and a sluggish electron-exporting efficiency between EABs and extracellular Cr(VI) within the natural EET pathway, as well as a low tolerance/resiliency of bacteria to withstand high Cr(VI) exposure. Therefore, more investigations are warranted to overcome the drawbacks of Cr(VI) removals strategies using traditional EABs. To increase the extracellular electron flux, novel artificial biohybrids may be fabricated by harnessing specific semiconductor nanoparticles (NPs) on the surface of an EAB's cell to harvest electrons generated by light illumination (Cestellos--Blanco et al., 2020; Fang et al., 2020). Since photoelectrons have a lower potential, they are more effectively accepted by Cr(VI) for reduction (Khare et al., 2018; Anand et al., 2019). As such, Cr(VI) reduction is enhanced by the synergistic cooperation between microbial reduction and photoelectric reduction in the presence of semiconductor NPs-coated biohybrids.

A variety of biohybrids have been successfully configured by pairing various host EABs with specific semiconductors (e.g., CdS, TiO_2 and InP NPs) (Dong et al., 2020a, 2020b). However, inherent defects in biohybrids assembled with metal-based semiconductors NPs often render them ineffective in application. For instance, a strong dependency on high-intensity light sources (e.g., UV-irradiation) for effective excitation of the metal-based semiconductor NPs having a wide range of band gaps creates a strong potential for damage to living cells (Svitkova et al., 2017). Further, high-intensity illumination may induce photocorrosion to the biohybrids assembling with metal-based semiconductor NPs and trigger leaching of toxic metals (Ding et al., 2019; Huang et al., 2019). Among a variety of nano-sized photosensitizers used for photocatalysis, the favorable properties of high water solubility, photostability and tunability of semiconducting carbon dots (CDs) are desirable when working with engineered advanced living biohybrids (Saini et al., 2020; Aggarwal et al., 2022). Further, positive surface charge and reducibility of amine-functionalized carbon dots (NCDs) provide added benefits to immobilize NCDs to surfaces of negatively charged bacteria and generate more reducing powers to aid Cr(VI) reduction (Guo et al., 2019; Thirumalaivasan and Wu, 2020). Thus, full exploitation of the intrinsic properties of NCDs has the potential to appreciably enhance the capabilities of living biohybrids for use in removal of Cr(VI) by reduction.

To improve the overall bioelectrochemical efficiency of biohybrids, modular configurations for all living/nonliving electron transfer machineries must be considered in constructing a reliable hybrid system that integrates a flexible conformational structure with sufficient energetic catalysis efficiency (Chen et al., 2022). Considering the orientation specificity of charge transport (Apetrei et al., 2019), the connections between living and non-living machineries in cell-semiconductor hybrid systems require a stable/efficient interfacial connector to optimize charge transduction similar to natural systems. This implies that formation of interfacial connector requires an extremely close and high surface area contact between cells and NCDs to maintain cellular viability and semiconductor properties (Sytnyk et al., 2017). Therein, employing charged polymers for layer-by-layer coating will create an effective configuration to sustain the compatibility between the abiotic and biotic components (Park et al., 2014; Nguyen et al., 2018). Thus, the engineered architecture should assure effective charge transport at interfacial connectors while also serving as an effective shield to sustain the survival of EAB cells.

Herein, we fabricated a living photosensitive biohybrid comprise of Cr(VI)-reducing bacteria, polydopamine (PDA) and NCDs in an inward-to-outward assembly configuration and evaluated its efficacy for removal of Cr(VI) by reduction in wastewaters. We further tested the applicability of the constructed living biohybrid incorporating a natural *Shewanella* genus under harsh environmental conditions with higher Cr (VI) exposure concentrations than previous investigated. The electron flux contributed from different pathways (e.g., biotic vs abiotic) and the production of cellular electron transfer machineries, such as outer-membrane c-type cytochromes (c-cyts), NADH/NAD^+ pool and flavins, were further determined to elucidate the mechanisms responsible for boosting the Cr(VI) reduction capacity of the biohybrid system.

2. Methods and materials

2.1. Cultivation of Cr(VI)-reducing strain

Prior to anaerobic Cr(VI) bioreduction experiments, a wild Cr(VI)-reducing strain of *S. oneidensis* MR-1 was cultured on a Luria–Bertani (LB) agar plate, then propagated using aerobic LB medium at 30 °C in a shaker (200 rpm) for 12 h. Throughout the entire incubation period, the biomass and cell density of bacterial cells were monitored on a dry cell weight basis and optical density at 600 nm (OD_{600}). The bacterial growth curve displaying OD_{600} value versus growth time is reported in Fig. S1. To measure dry cell weight, 1.0 mL of bacterial fluid was extracted from the inoculums and centrifuged at 5000 g for 3 min to harvest the cell cluster. The cell cluster was washed three times with deionized water and dried (60 °C) to constant weight. The correlation between dry cell weight and OD_{600} is shown in Fig. S2.

2.2. An inward-to-outward construction of concrete cells

The procedure for inward-to-outward assembly of NCDs to *S. oneidensis* MR-1 (denoted as SW) cells was divided into three steps: (1) intracellular internalization with NCDs, (2) PDA-coating at abiotic/biotic junction interfaces, and (3) NCDs-anchoring to the outermost shell (Fig. 1). The NCDs (band gap at 2.31 eV and average size of 1–3 nm) were purchased from Janus New-Materials Co., China. The procedure for intracellular internalization with NCDs followed by Liu et al., (2020) and Yang et al., (2020). In brief, 204 μL wild strain enrichment was aerobically activated in 20 mL LB medium (which contained 100 mg/L NCDs) at 30 °C in a shaker (200 rpm in the dark) for 16 h to obtained a NCDs-internalized bacteria-rich fluid (denoted as ISW cells and $OD_{600} \approx$ 1.8). Then, the proliferated cells were harvested through centrifugation at 5000 g for 5 min and re-suspended in 1.0 mL Bis-Tris propane (BTP) (10 mM, pH 7.0) with a high purity nitrogen atmosphere for 30 min. Next, 1.0 mL of 4.0 g/L PDA was added to the anaerobic bacterial resuspension for in-situ polymerization (denoted as ISW@PDA cells). Finally, 0.245 mL of 2.0 g/L NCDs stock solution was injected into ISW@PDA mixtures and purged with a nitrogen atmosphere for 2 h at 30 °C in the dark to harvest the hybrid cells that were coated on the NCDs-shell (denoted as ISW@PDA@NCDS cells). The resulting biohybrids were collected by centrifugation at 5000 g for 3 min and washed two times with 2.0 mL BTP solution (10 mM). To examine the

survivability of different concreted cells, an equal density of biomasses (OD_{600} ≈ 0.3) were transferred to Cr(VI)-free anaerobic mediums (which contains 20 mM lactate, and the compositions are listed in Table S1) for a 72 h proliferation period at 30 °C in the dark. The OD_{600} values for each treatment were recorded over time to contrast the growth rates of the different engineered strains.

2.3. 2.3 assays design

We used a higher Cr(VI) exposure level than previous investigations to determine toxicity impacts on the *Shewanella* genus. An initial concentration of 100 mg/L Cr(VI) was used for the toxicity assays, which was twice that of the maximal suitable Cr(VI) concentration deemed survivable by the *Shewanella* genus in previous studies (Li et al., 2019, 2020; Luo et al., 2019). To investigate the efficacy of Cr(VI) removal by different concreted cells under given illuminated conditions (light vs dark), batch experiments were conducted by incubating a given biomass (corresponding to OD_{600} ≈ 0.3) in 40.0 mL anaerobic medium containing 100 mg/L Cr(VI) in 50.0 mL serum bottles. In detail, the biotic assays were amended with (1) SW cells + dark, (2) ISW@PDA@NCDs cells + dark, (3) SW cells + illumination, and (4) ISW@PDA@NCDs + illumination. Additionally, abiotic assays were conducted by incubating with inactivated cells under otherwise parallel incubation conditions. Each amendment was performed in triplicate and cultured at 30 °C. Thus, a total of 24 samples were in turn incubated in biotic (12 samples) and abiotic (12 samples) amendments. All amendments were deoxygenated with high purity N_2 atmosphere for 60 min: the first 30 min into the liquid phase and another 30 min into the headspace above the liquid phase; then the bottles were sealed.

Prior to usage, inactivated cells and sterile anaerobic mediums were deoxygenated with high purity N_2 for 1 h and then autoclaved for 20 min at 120 °C. All incubation and procedures were strictly anaerobic and performed in an anaerobic glovebox. To create a platform for visible-light photocatalysis, a visible light source was supplied with white LED belt irradiation, with an approximate light energy of 80 μmol/m^2·s. Throughout the entire incubation period, aliquots of approximately 2.0 mL supernatant were extracted using a sterilized syringe and then pass through a 0.22-μm filter (polyethersulfone, Jinteng Co., Ltd, China) to quantify concentrations of Cr(VI), Cr(T) (total chromium), DOC and biomass. The sampling processes were also conducted in an anaerobic glovebox.

2.4. 2.4 Analytical methods

2.4.1. Determination of Cr and DOC

Concentrations of Cr(VI) and Cr(T) were determined using the 1,5-diphenylcarbazide (DPC) spectrophotometric method and ICP-MS (NexION, 2000; PerkinElmer, USA), respectively (Han et al., 2017). Prior to analysis, 1.5 mL supernatant was extracted from serum bottles using a sterilized injector and then filtered through a 0.22-μm filter. Further, the precipitate deposited at the bottom of serum bottles was collected and washed twice using 70% ethyl alcohol and then vacuum-dried to identify the speciation of Cr using a Quantum-2000 (USA) X-ray photoelectron spectroscopy microprobe (Mullet et al., 2007). The dissolved organic carbon extracted from the supernatant was measured using a TOC analyzer (Shimadzu, TOC-L CPH, Japan) to estimate the degradation of organic carbon that was associated with the supply of bio-electrons and photoelectrons. Prior to determination of DOC, the supernatant was filtered through a 0.45 μm membrane filter (Millipore, USA).

2.4.2. Determination of c-cyts

Outer-membrane c-cyts of EABs serve as critical carriers for directly transporting intracellular electrons to extracellular electron acceptors (Richardson et al., 2012; Liu et al., 2015). Our previous findings also demonstrated that heterojunctions of specific carbon-based nanomaterials (such as graphene) could up-regulate the expressions of specific c-cyts of EABs (Li et al., 2020). Herein, the total production of c-cyts for SW, ISW and ISW@PDA@NCDs cells was determined using the protocols for the c-cyt ELISA Kit (Shanghai Lanpai Biotechnology, China) (Dong et al., 2021). Briefly, a 10 μL test sample and 40 μL sample diluent were firstly added in a 96-well plate and then mixed using a homogenizer for 3 min. Thereafter, the resulting mixture in each well received 100 μL of HRP-conjugate reagent, covered with an adhesive strip and incubated at 37 °C for 60 min. Then the samples were rinsed 5 times with Mili-Q water (400 μL per time) while ensuing a complete removal of liquid after each rinse. Chromogen solutions A (50 μL) and B (50 μL) were then added to each well, gently mixed and incubated for 15 min at 37 °C in the dark. Next, c-cyts production of all samples was recorded within 15 min using a microtiter plate reader (PerkinElmer, EnSpire, USA) and quantified according to the standard curve for c-cyts concentration versus OD values at 450 nm. Finally, the production of c-cyts was normalized to the weight of biomass in each amendment.

2.4.3. Quantification of extracellular flavins

Electrically active redox flavin compounds secreted by *Shewanella* genera are a key factor accelerating extracellular electron transport in a cyclic fashion through shuttling electron transfers between the cell surface and substrate (Brutinel and Gralnick, 2012). Hence, the secretion of extracellular flavins from modified *S. oneidensis* MR-1 in different concreted systems were quantified. Flavin production was monitored using a fluorescence spectrophotometer (FS5, Edinburgh, UK) (Sivakumar et al., 2014). Approximately 1.0 mL of bacterial fluid from each concrete preparation system (illustrated in section 2.2) was extracted and centrifuged at 12,000 *g* for 10 min at 4 °C. Flavin compounds in the supernatant were measured by determining the fluorescence intensities of the maximal emission peak at 525 nm by fixing the excitation wavelength at 440 nm. Next, the fluorescence intensity of the anaerobic

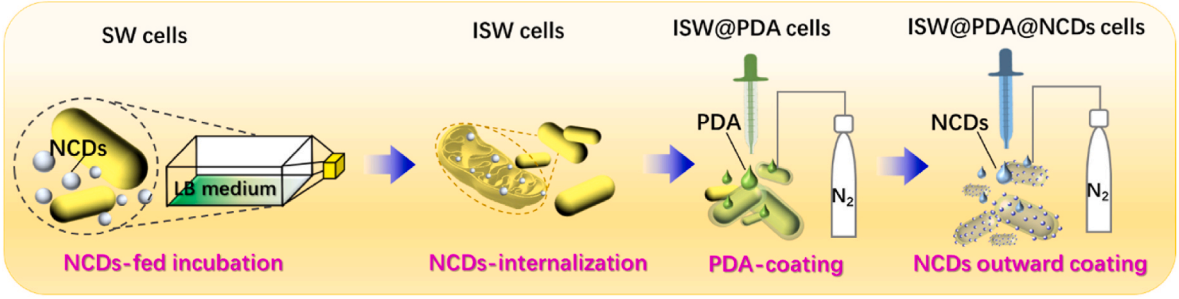

Fig. 1. Schematic for the fabrication of living photosensitive biohybrids in an inward-to-outward assembly of NCDs and PDA, in which *S. oneidensis* MR-1 cells are firstly internalized with NCDs in LB medium culture at 30 °C for 16 h. Then, PDA-coating was conducted to NCDs-internalized bacteria-rich fluid under N_2 atmosphere. Finally, NCDs-outward configuration was carried out by adding 0.245 mL of 2.0 g/L NCDs stock solution into ISW@PDA mixtures and purged under N_2 atmosphere for 2 h at 30 °C in the dark.

medium was used as a blank control to eliminate the fluorescent disturbance from background substrates. Finally, the production of flavins was reported on a per unit weight of biomass basis for all amendments.

2.4.4. Quantifications of intracellular NADH and NAD $^+$ levels

Intracellular NADH and NAD^+ levels in raw SW and ISW@PDA@NCDs cells were quantified at time 0 and 48 h during the incubations according to protocols for the NAD(H) Quantification Assay Kit (Bioss Co., China). In brief, 5 mL bacterial fluid was collected by centrifugation (10,000 *g* at 4 °C for 5 min) and immediately re-suspended in 1.0 mL of acid extract (for NAD^+) or alkaline extract (for NADH) (Yong et al., 2014; Li et al., 2018a). The re-suspended mixtures were firstly ultra-sonicated at 20% intensity for 1 min in an ice-bath, then heated with cap sealed at 95 °C for 5 min, and finally collected by centrifugation (10,000 *g* at 4 °C for 10 min) after cooling in an ice-bath. Next, 500 μL supernatant from the previous step was neutralized with 500 μL alkaline extract (for NAD^+) or acid extract (for NADH), then fully homogenized, and collected by centrifugation (10,000 *g* at 4 °C for 10 min). The final supernatants were stored in an ice-bath to determine the levels of NAD^+ and NADH by using an ultraviolet and visible spectrophotometer. Additionally, cell concentrations for each NAD^+ and NADH sample were was detected by plate counts on LB agar (Li et al., 2018a).

2.5. Data analysis

A pseudo-first order reaction kinetic model was employed to describe Cr(VI) reduction rates as shown in Eq. (1), where k is the first-order rate constant. Cr(VI) reduction efficiency (u) was calculated to report the average Cr(VI) removal degree by individual cells and reaction time (Eq. (2)). C_0 and C_t are the Cr(VI) concentrations at time O and t, while t and m are the incubation times and corresponding accumulated biomass, respectively. DOC loss per unit biomass for SW and ISW@PDA@NCDs cells involved in the processes of photodegradation & physical adsorption (T_p) and microbial consumption (T_m) was used to estimate the degradations of organic carbon associated with the supply of bio-electrons and photoelectrons. The respective relative DOC contributions were weighted according to Eq. (3) and Eq. (4). T_0' and T_t' are the DOC concentrations at time O and t during the biotic assays incubated with a given inoculum (i.e., SW or ISW@PDA@NCDs cells) under a given illuminated condition (i.e., light or dark). Similarly, T_0 and T_t are the DOC concentrations at time O and t in the abiotic assays using the same inoculum under the same illuminated conditions as with the biotic assays.

$$k = \frac{LnC_0 - LnC_t}{t} \tag{1}$$

$$u = \frac{C_0 - C_t}{m \times t} \tag{2}$$

$$T_p = \frac{T_0 - T_t}{m} \tag{3}$$

$$T_m = \frac{(T_0^{'} - T_t^{'}) - (T_0 - T_t)}{m} \tag{4}$$

Data were analyzed and visualized using Origin 9.0, Microsoft Excel 2016 and SPSS 20.0 software. Each data point represents the average value of at least three measurements. The standard deviations of the triplicate analyses were reported as error bars in the corresponding graphs. Statistical comparisons were determined by analysis of variance using SPSS with a 95% confidence level ($P < 0.05$).

3. Results and discussion

3.1. Characterization of living ISW@PDA@NCDs biohybrids

Bacterial fluids cultured in NCD-containing LB medium and the PDA-NCDs mixed dispersion culture system were characterized by TEM and SEM observations. Compared to SW cells in the control sample (Fig. 2e–f), TEM characterization (Fig. 2g–h) showed that NCDs were densely implanted into the intracellular membranes of ISW cells, revealing a successful internalization of NCDs in bacterial intracellular interfaces. Measurement of micro-dimensions by TEM indicated a precise match of particle size with the NCD size, confirming the concretion of NCDs into cells (Fig. 2h). SEM image of ISW@PDA cells is depicted in Fig. 2c and reveals that a unique shell-like structure created by PDA is coating the surface of the outer membrane (Fig. 2a–b) of bacterial cells. Further, SEM and TEM images (Fig. 2d and j) of ISW@PDA@NCDs cells showed a large number of tiny NCD nanospheres were densely inlaid into the PDA layer, demonstrating a successful formation of dual shells incorporating a PDA layer and NCDs with ISW@PDA cells (Fig. 2c and i). The color (Fig. 2k) of ISW@PDA@NCDs bacterial fluids was similar to that of the blue-emission NCDs under purple light irradiations, compared to the contrasting colors in ISW (violet) and SW (purple) samples. These results substantiate the successful configuration of the ISW@PDA@NCDs biohybrid.

Surface modifications of bacterial cells were apparent in changes to bacterial surface charge. Zeta potential measurements show that NCD-concretion to bacterial cells increased positive charge on bacterial surfaces (Table S2), owing to a shift from -27.8 ± 2.5 mV (SW cells) to -11.8 ± 1.2 mV (ISW@PDA@NCDs cells). Different hybrid bacterial fluids with the same initial biomass were injected into a Cr(VI)-free anaerobic medium to test the survival/growth of different concreted cells. Throughout the 72-h anaerobic incubation, the configurations of NCDs and/or PDA appeared more favorable to the growth of the concreted cells compared to the growth trend of natural SW cells (Fig. S3). Notably, the treatment with NCD-internalization was most favorable to bacterial growth among all treatments. This favorable tendency is likely associated with enhanced metabolism due to the presence of NCDs (Yang et al., 2020).

3.2. Cr(VI) removal by concreted cells with illumination

Among the eight treatments, Cr(VI) removal in illuminated treatments was sharply increased compared to that of dark treatments (Fig. 3a and Fig. S4). More than 50% of Cr(VI) was removed within 72 h in the illuminated assays. This compares to a maximum Cr(VI) removal efficiency in dark treatments of only 37% after 192 h. These results stress the importance of photoreduction in the removal of Cr(VI) (Bhati et al., 2019). Under the same illuminated conditions, microbial reduction gave a distinct boost to Cr(VI) reduction. For instance, the treatment with illumination plus with active bacterial cells result in 0.4–0.6 fold of enhancements in Cr(VI) reduction than that of abiotic assays, and nearly 0.4–0.8 fold of enhancements in Cr(VI) reduction are also achieved by the dark treatment with active bacterial cells. Further, NCD-concretion promoted Cr(VI) removal compared to NCD-free assays. Notably, treatment with ISW@PDA@NCDs plus illumination exhibited the highest capacity for Cr(VI) removal among all treatments, with a virtually complete removal (100%) after 72 h. The removal kinetics followed a pseudo-first-order reaction rate with a rate constant of 0.0373 h^{-1} (depicted in Fig. 3a–b).

Extremely poor Cr(VI) removal of only 2.5% was achieved in pure strain-incubated assays under dark conditions. In contrast, the sterile ISW@PDA@NCDs biohybrids in the dark contributed appreciable reducing powers for Cr(VI) reduction and surprisingly outperformed the ability of active SW cells with a Cr(VI) reduction performance up to 3.5 times that of active SW cells in the dark. We ascribe this performance enhancement to the concretions having a positive charge and the

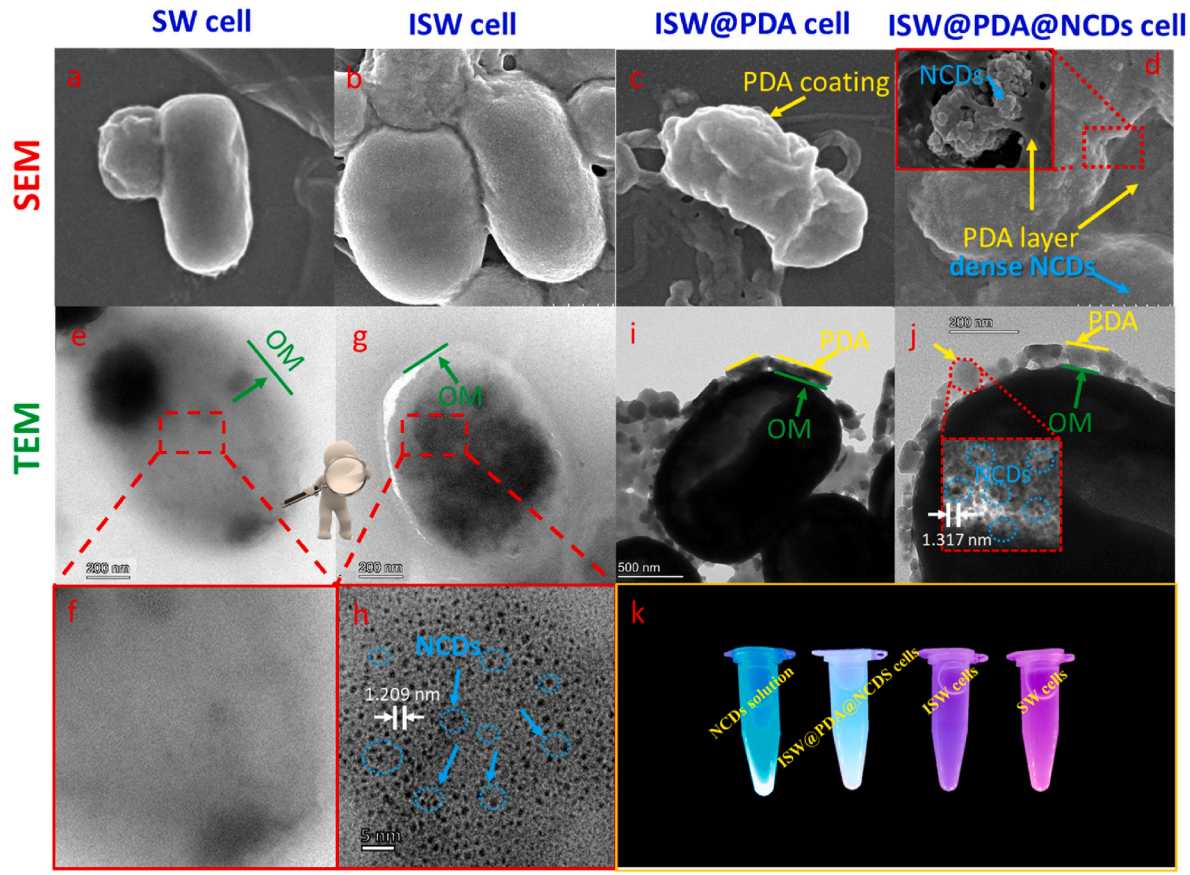

Fig. 2. SEM images of SW cell (a), ISW cell (b), ISW@PDA cell (c) and ISW@PDA@NCDs cell (d). TEM images of SW cell (e and f), ISW cell (g and h), ISW@PDA cell (i) and ISW@PDA@NCDs cell (j). A color comparison (k) for the bacterial fluids resulting from different concretions under purple light irradiation. The yellow, blue and green arrows indicate the presence of PDA layer, NCDs and outer membrane (OM), respectively. (For interpretation of the references to color in this figure legend, the reader is referred to the Web version of this article.)

reductive capacity of NCDs in ISW@PDA@NCDs biohybrids inducing adsorption of the Cr(VI) anion and a rapid reduction of Cr(VI) facilitated by the reductive capacity of NCDs. Thus, the unique hybrid structures endowed within ISW@PDA@NCDs biohybrids generate a greater bulk electron flux to facilitate the reduction/removal of Cr(VI).

Based on the trends for Cr(T) removal, a comparable high removal (nearly 18–53%, shown in Fig. 3c) of soluble Cr(T) was found in the presence of ISW@PDA@NCDs biohybrids, regardless of abiotic or biotic conditions. Since the NCD-derived shell in biohybrids is positively charged (Table S2), negatively charged Cr(VI) anions are absorbed to biohybrids through electrostatic adsorption. The Cr(T) concentrations were also sharply decreased in illuminated systems. This infers that photoreduction is involved in the rapid conversion of soluble Cr(VI) to insoluble Cr(III) precipitates. The solid-phase precipitates separated from the ISW@PDA@NCDs biohybrids plus illumination treatment were characterize to determine the oxidation/coordination status of Cr using XPS. A pair of representative peaks located at 579.3 and 585.4 eV for Cr^{3+} 2p3/2 and Cr^{3+} 2p1/2 (Fig. 3d) displayed a downward shift in the Cr 2p spectra (Li et al., 2019), demonstrating that the initially present Cr (VI) was substantively transformed to Cr(III). These results demonstrate that ISW@PDA@NCDs biohybrids offer distinct advantages compared to SW, namely a higher Cr(VI) reduction ability and a stronger survival tolerance to higher Cr(VI) exposure concentrations (>50 mg/L).

3.3. Enhanced Cr(VI) reduction efficiency by ISW@PDA@NCDs cells

Based on changes in OD_{600} values, hybrid concretions promoted bacterial growth compared to their respective control groups under the same illumination conditions (Fig. 4a). This might result from the specific shell structure of biohybrids offering a protective effect to SW cells (Song et al., 2017). Moreover, bacterial growth may be influenced by exposure to high Cr(VI) concentrations. Since Cr(VI) reduction was greater in illuminated versus dark treatments (Fig. 3a), the resulting lower Cr(VI) concentrations in illuminated treatments will reduce potential toxicity impacts. The reduction in toxicity potential provides a more favorable habitat for bacterial survival and reproduction in illuminated versus dark treatments. This inference is supported by the higher OD_{600} values in the illuminated treatments.

The Cr(VI) reduction efficiency was calculated per unit biomass (Fig. 4b) to demonstrate that the enhanced Cr(VI) reduction was related to differences in the Cr(VI) reduction capability of specific individual cells rather than a greater bacterial biomass. Therein, the overall trend for Cr(VI) reduction efficiency among the four biotic amendments followed the order: ISW@PDA@NCDs (light) > SW (light) > ISW@PDA@NCDs (dark) > SW (dark). Specifically, the maximum Cr(VI) reduction efficiency of the ISW@PDA@NCDs (light) treatment was 1.6, 2.6 and 4.1 times higher than that of the SW (light), ISW@PDA@NCDs (dark) and SW (dark) treatments (Fig. 4c), respectively. Collectively, the high first-order rate constant and Cr(VI) reduction efficiency displayed by the illuminated ISW@PDA@NCDs biohybrids (Figs. 3b and 4c) demonstrate the prominent performance of illuminated ISW@PDA@NCDs biohybrids to generate a high bulk electron flux and rapidly transfer these electrons for Cr(VI) reduction.

3.4. Energy harvesting by ISW@PDA@NCDs cells in dark versus illuminated conditions

To examine electron flux contributions from abiotic versus biotic

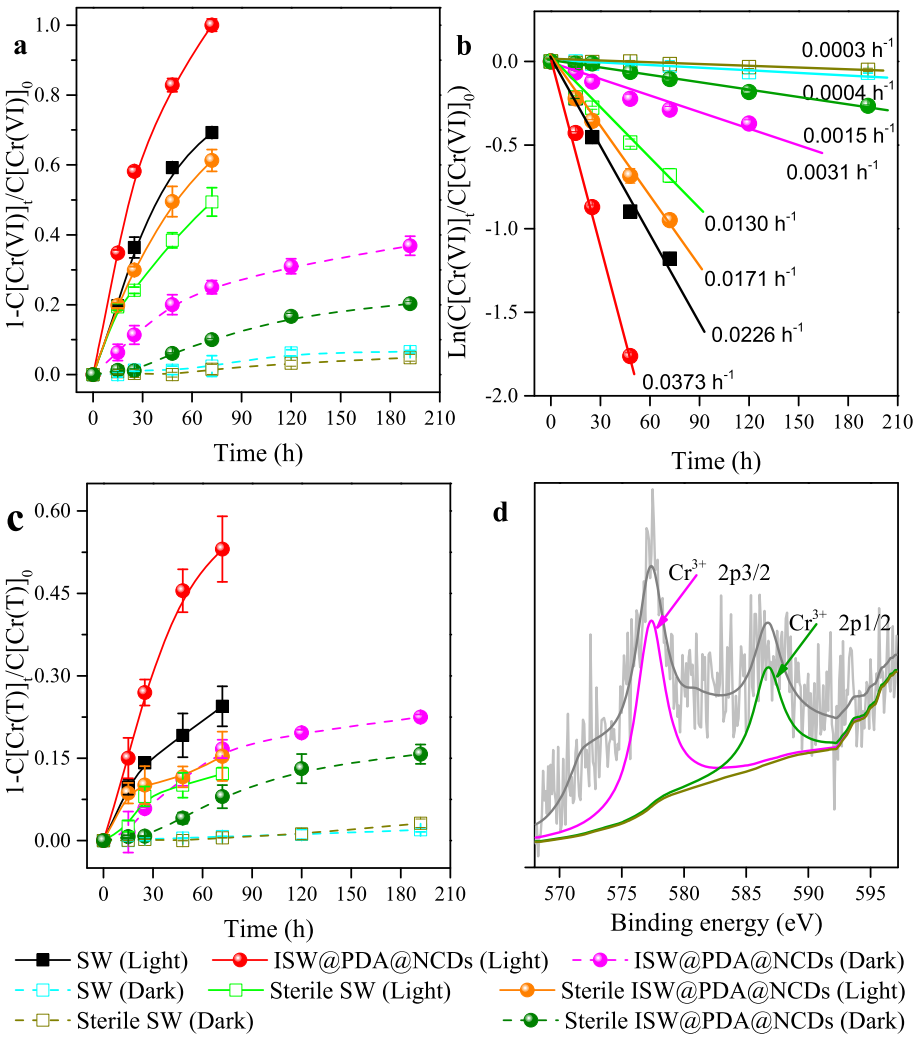

Fig. 3. Removal dynamics of Cr(VI) (a), pseudo-first-order kinetic fitting of Cr(VI) removal (b) and Cr(T) removal dynamics (c) by treatments with active/inactive SW or ISW@PDA@NCDs cells with or without visible light illumination (n = 3; error bars indicate SD). XPS characterization of Cr 2p (d) for precipitates collected from assays incubated with active ISW@PDA@NCDs cells under light illumination.

pathways, the consumption of DOC was measured for all amendments (Fig. 5a). Very limited removal (1.4–3.4%) of DOC occurred in abiotic treatments compared to that of biotic treatments (3.2–12.5%). For active ISW@PDA@NCDs and SW cells, DOC consumption was higher in the dark than under illuminated conditions. Among biotic treatments, DOC consumption for the ISW@PDA@NCDs samples under illuminated and dark conditions represented opposing extremes. Based on the 72 h sampling time, DOC consumption by ISW@PDA@NCDs was up to 12.5% in the dark, whereas DOC consumption was only 4.4% under illumination. By contrasting with respective active control groups, the consumption of organic substrate is starkly decreased by 52% in illuminated active biohybrid cells, whereas the consumption is increased by 18% in dark condition. A remarkably increased consumption may be attributed to an intensive metabolism enhancement including intracellular charge production, ATP level and extracellular secretion due to the NCDs-fed treatment (Yang et al., 2020).

We further calculated the DOC consumption by active SW or ISW@PDA@NCDs cells on a per unit biomass basis after incubating for 72 h (Fig. 5b). In terms of relative consumption of DOC by microbial metabolism, ISW@PDA@NCDs cells incubated in the dark showed the highest dependency on DOC consumption (nearly 1.5-fold of SW cells incubated in the dark), whereas the dependency on DOC consumption by illuminated ISW@PDA@NCDs cells was only 25% that of the illuminated SW cells. Under illuminated conditions, photodegradation of organic substrates in the anaerobic medium contributed a limited electron flux, as inferred from the similar DOC consumption by illuminated ISW@PDA@NCDs and SW cells. This implies that the enhanced Cr(VI) reduction was attributable to more photoelectrons and reducing powers supplied from the illuminated NCDs. These findings indicate that ISW@PDA@NCDs cells exhibit a unique flexibility in harvesting energy as a function of illumination to facilitate in the Cr(VI) reduction process. Hybrid concretions stimulated microbial metabolism processes in SW cells to produce bio-electrons in the dark to participate in Cr(VI) reduction, whereas illuminated ISW@PDA@NCDs cells preferentially utilized photoelectrons for Cr(VI) reduction.

3.5. *Increased production of c-cyts and flavins in ISW@PDA@NCDs cells*

The enhanced Cr(VI) reduction rates by ISW@PDA@NCDs cells (supported by Fig. 4b) indicate a mechanism for accelerated electron transport in ISW@PDA@NCDs cells. Intracellular c-cyts may serve as an important transmembrane electron-export carrier and extracellular flavins may enhance shuttling of inward-to-outward delivered electrons (Lin et al., 2018; Heidary et al., 2020). Consistent with the finding by Yang et al., (2020), the production of c-cyts was significantly up-regulated by 2.2- and 5.7-fold in ISW and ISW@PDA@NCDs cells compared to SW cells (Fig. 6a). Likewise, higher flavins (Fig. 6b) were secreted by ISW@PDA@NCDs cells (increased by 0.7-fold versus SW

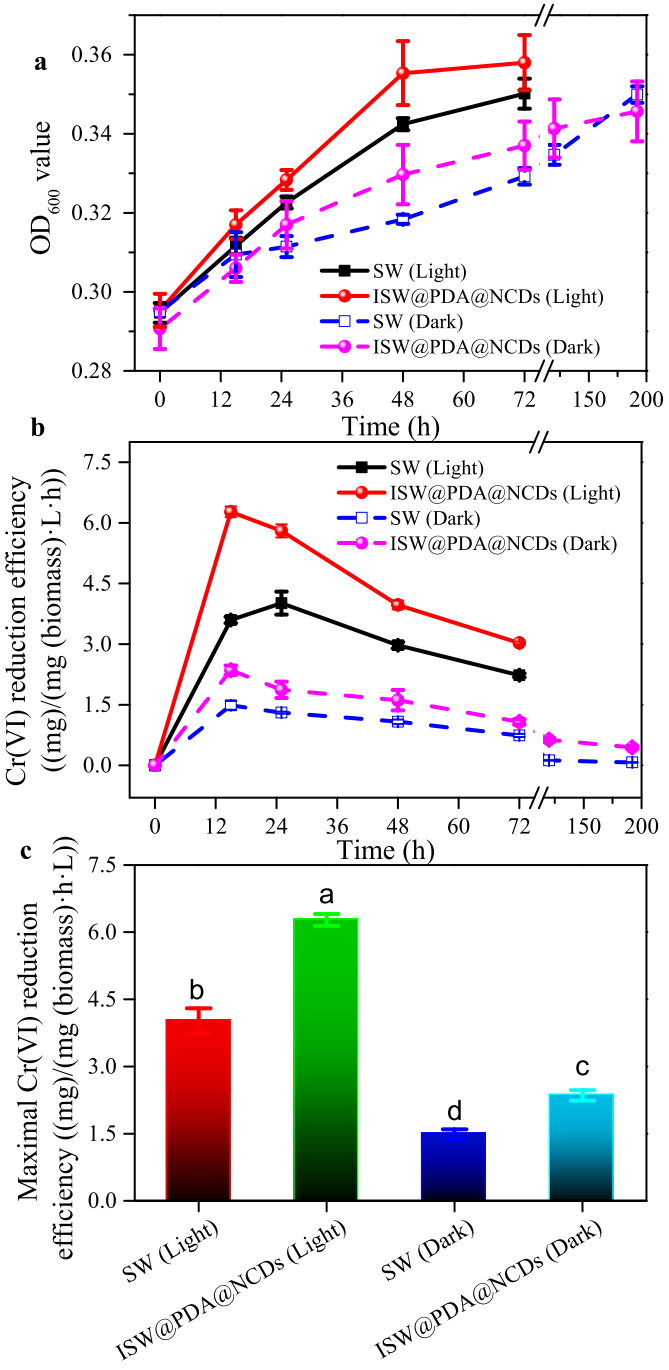

Fig. 4. Based on the entire incubation period, changes in OD_{600} values (a), Cr (VI) reduction efficiency calculated on a per unit weight biomass basis (b) and the maximum Cr(VI) reduction efficiencies (c) for SW and ISW@PDA@NCDs cells with or without light illumination (n = 3; error bars indicate SD); different lower case letters indicate treatment are significantly different at $P < 0.05$.

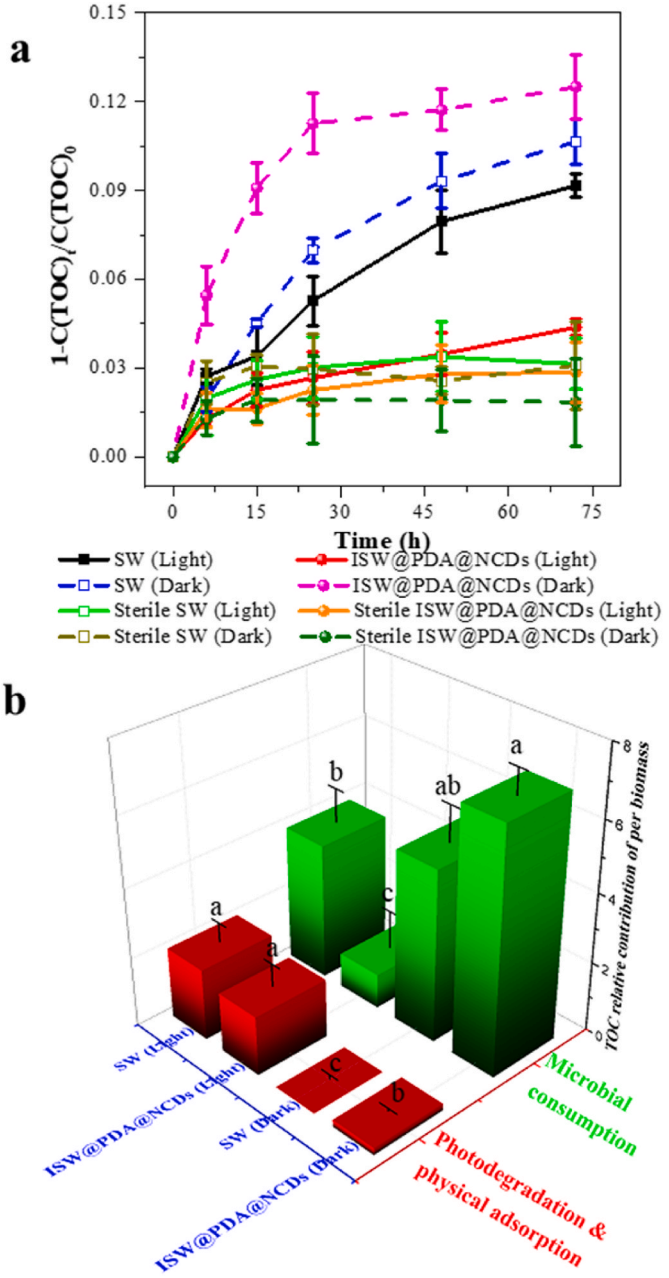

Fig. 5. Overall consumption (a) of TOC by treatments of active/inactive SW or ISW@PDA@NCDs cells with or without light illumination (error bars indicate SD). Mean ± SD (b) of the relative contribution of TOC per unit biomass for SW and ISW@PDA@NCDs cells that were incubated for 72 h with or without light illumination (n = 3); different lower case letters among treatment groups indicate a significant difference at $P < 0.05$. Herein, the TOC from microbial consumption by illuminated ISW@PDA@NCDs cells was set as the reference value of 1.

cells), which is likely due to the PDA-coating that adsorbs extracellular flavin molecules (Liu et al., 2019a). Conductive NCDs may promote charge transfer at junction interfaces providing a more conductive pathway (Dhenadhayalan et al., 2020). Thus, multiple reinforcements at interfacial connectors harness more electron-transfer conduits, that in turn attenuate electron escape or sluggish electron-transfer/export across the complicated abiotic/biotic interfaces between engineered cells and extracellular Cr(VI). Moreover, the increased productions of c-cyts and flavins may also allow the coordination of electron-exporting at both internal and external sides of membranes, creating a long-range EET network/pathway in those electron-transfer conduits where conductive c-cyts are closely bound to outer-flavins (Li et al., 2018c).

3.6. Increased intracellular reducing equivalents by an enlarged NADH/NAD^+ pool

Since NADH and NAD^+ are the pivotal cofactors participating in microbial metabolism of organic substrates, they serve as important intracellular electron carriers and sources in EET processes (Chen et al., 2014; Yong et al., 2014). Hence, enlarging the NADH/NAD^+ pool would

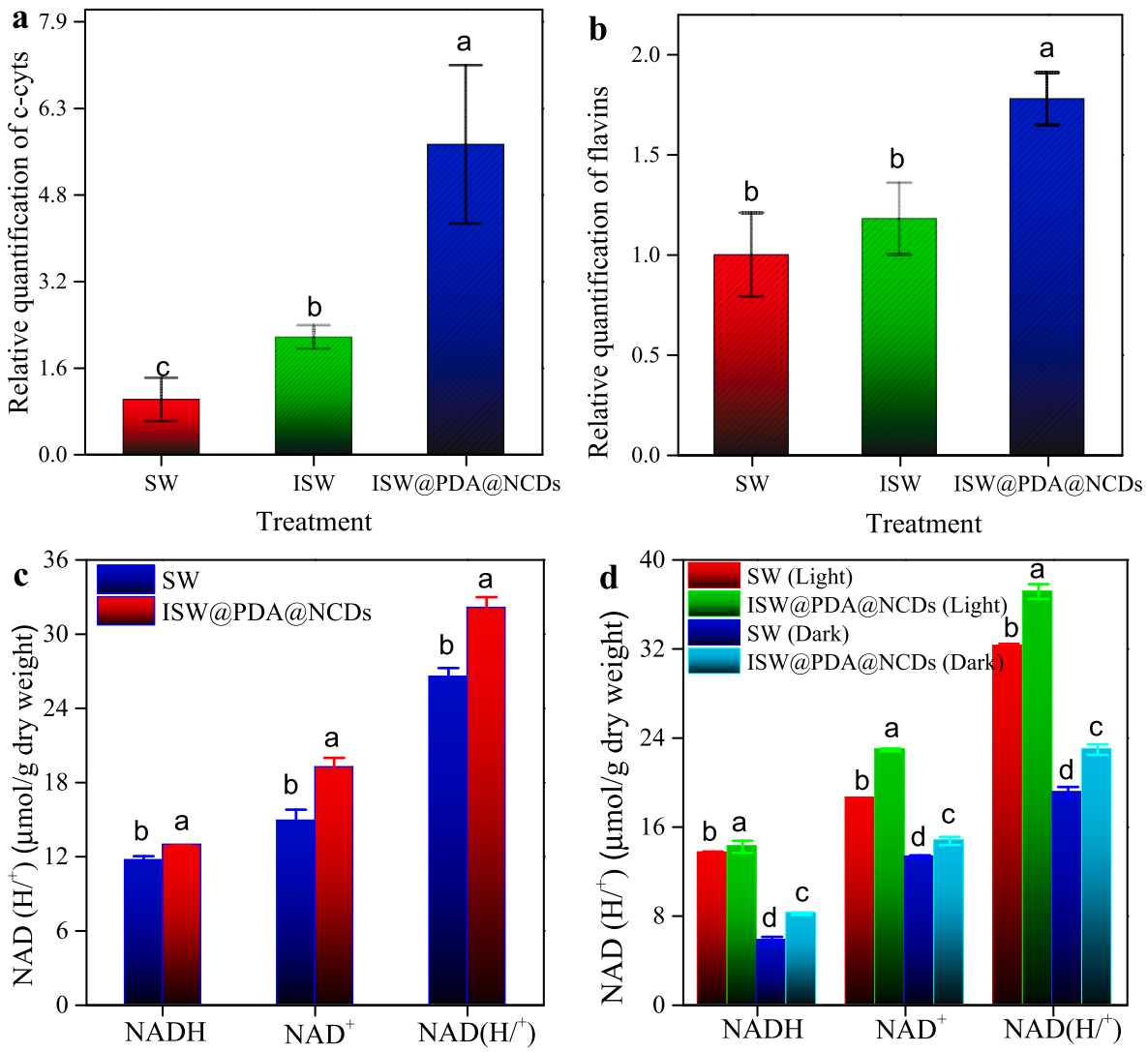

Fig. 6. Production levels (mean ± SD) of intracellular c-cyts (a) and extracellular flavins (b) in different concreted cells (n = 3); concentrations (mean ± SD) of NADH, NAD^+ and $NAD(H/^+)$ for SW and ISW@PDA@NCDs cells at the start of the incubation (c) and after 48 h of incubation with or without light illumination (d) (n = 3); different lower case letters among treatment groups indicate a significant difference at $P < 0.05$.

be expected to enhance the intracellular electron flux delivered to the outer membrane. We found that the intracellular NAD^+, NADH, and $NAD(H/^+)$ concentrations were increased in the ISW@PDA@NCDs cells compared to raw SW cells (Fig. 6c). This augmented effect for ISW@PDA@NCDs cells was also verified in subsequent 48 h-incubations conducted under the same illumination conditions (Fig. 6d). The impact of illumination on NADH/NAD^+ levels expressed in SW or ISW@PDA@NCDs cells showed a similar pattern to the trends for Cr(VI) reduction rates (Fig. 4b–c). Compared to SW cells in the dark, ISW@PDA@NCDs cells had a 1.1-fold increase in the intracellular NAD^+ level, which consequently increased the regeneration of NADH (a typical carrier of intracellular electrons) by 1.4-fold. Notably, NADH, NAD^+ and NAD ($H/^+$) levels were augmented 2.5-, 1.7- and 2.0-fold in illuminated ISW@PDA@NCDs cells, respectively, compared to that of SW cells incubated in the dark. The enlarged capacity of NADH/NAD^+ pool in biohybrid system after light illumination showed a similar trend with the performance of Cr(VI) bioreduction under the same illuminated condition (Fig. 4b–c). These findings suggested that the photoelectrons generated by NCDs under light irradiation could be transferred to bacteria, leading to the production of NADH, a reducing equivalent for the biosynthetic reactions leading to Cr(VI) reduction.

As microbial metabolism depends on organic substrates, the main intracellular reducing equivalents are primarily delivered to cofactor-oxidized NAD^+ to generate the reduced form of NADH. The NADH then serves as a major releasable intracellular electron carrier and contributes to microbially-facilitated reduction reactions (Wang et al., 2017). With a vigorous actuation of intracellular cofactors, an outward transport of electrons is facilitated, owing to the excessive intracellular reducing equivalents that were originally stored in lactate (Li et al., 2018b). We found an increased size of the $NAD(H/^+)$ pool that triggered a high efficiency NADH regeneration and correspondingly donated more releasable intracellular electrons that were supplied from NADH-dependent pathways. Hence, the enhanced Cr(VI) reduction found in the presence of illuminated ISW@PDA@NCDs cells might be partially contributed by the elevated intracellular reducing equivalents. Improvements in the intracellular redox balance on the headend would be expected to contribute to the performance of EET processes on the backend.

3.7. *Mechanisms for visible light-enhanced microbial-photoreduction of Cr(VI)*

To the best of our knowledge, this is the first example of a successful modification of the *Shewanella* genus to develop a high-efficiency,

microbial-photoreduction system for Cr(VI) in which the modified cells are able to survive/function at Cr(VI) concentrations greater than 50 mg/L. Compared to previous investigations (Table 1), we developed a novel *S. oneidensis* MR-1 biohybrid with high-efficiency Cr(VI) reduction capacity at Cr(VI) concentrations up to 100 mg/L. Especially using an incubation with a comparably lower biomass to withstand a higher Cr (VI) exposure, our study achieved a higher Cr(VI) reduction effect (up to 100%) versus most of other peer works (are mostly below 50 mg/L). Although the reduction efficiency (1.4 mg/(L·h)) was lower than that (5.2 mg/(L·h) of some peer works integrating with illumination, a stronger adaptability with a lower biomass derived from our methodology is considered more superior than that of peer works. Mitigation of Cr(VI) cellular toxicity is ascribed to multiple protection strategies associated with the chassis of living biohybrids that are supported from a PDA-coated shell and direct reduction and/or indirect photoreduction of Cr(VI) mitigating injury. The high Cr(VI) reduction efficiency of our biohybrid system was superior to recent published studies, and demonstrates strong efficacy for use in harsh environments contaminated with high Cr(VI) levels. Overall, the design of living photosensitive biohybrids for high yield/efficiency electron generation and transport to strengthen Cr(VI) reduction encompass (i) the liberations of intracellular electrons, (ii) foreign supply of extracellular reducing powers, and (iii) flexible modulation of charge transport at junction interfaces (Fig. 7a).

Overall, the mechanism of visible light-enhanced microbial-photoreduction of Cr(VI) in the presence of ISW@PDA@NCDs biohybrids is illustrated in Fig. 7b. Since quantum sized and positively charged NCDs are easily anchored into cytoplasm, periplasmic membranes or pili of SW cells (Guo et al., 2019; Liu et al., 2020), conductive NCD-internalization ensures rapid charge transport across NCD-tethered hybrid orbits (Kortemme et al., 2003; Der et al., 2012). With increased expression of c-cyts in NCD treatments, intrinsic sluggish electron transport in the original dynamic protein is liberated through more conductive c-cyts-NCD junction channels (Ha et al., 2021). With elevated levels of intracellular NADH/NAD^+, intracellular and extracellular Cr(VI) reduction is facilitated due to an enhancement of inward-to-outward transport of more releasable reducing equivalents. Thus, optimization of the NCD-internalized biological chassis fills the gaps originally lacking in sufficient intracellular protein-cyt c complexes, redox carriers and/or reducing equivalents in natural cells. These characteristics create an efficient transmembrane electron-export capacity, as well as docks for subsequent extracellular reaction processes. Next, extracellular Cr(VI) reduction pathways are launched through acceptance of photoinduced electrons, illuminated NCD-produced photoelectrons and bio-electrons, as well as NCD-induced direct reduction. Due to the dense NCD surface coating and increased production of extracellular flavins, additional electron-exporting conduits and electron-shuttling orbits are harnessed within living biohybrids.

The biocompatible PDA layer serves as a key abiotic-biotic junction connector within the biohybrid architecture. It not only creates a bulk shell to immobilize NCDs, but it also offers a protective shield to immediately scavenge photo-holes, which helps biohybrids resist damage from ROS. This unique self-defensive system endows ISW@PDA@NCDs biohybrids with greater resiliency/adaptability without adding any sacrificial agents (such as cysteine), which are frequently added to quench photo-holes in many conventional semiconductor NP-assembled biohybrids (Sakimoto et al., 2016). Further, the PDA-coating retains extracellular flavins, which might initiate a unique electron transport channel connected by double mediators (PDA and flavin) (Liu et al., 2019a). Hence, more efficient and biocompatible electronic configurations at intracellular/extracellular interfaces generate an efficient configuration framework and provide synergist potentials to ISW@PDA@NCDs biohybrids, wherein each component (abiotic and biotic) contributes respective advantages while offsetting respective weaknesses. A highly effective microbial-photoreduction system adaptable to harsh Cr(VI) exposure is the result of this synergetic relationship. The resulting ISW@PDA@NCDs cells integrate multiple functions between the abiotic/biotic components making them highly efficient for Cr(VI) reduction, with the potential for adaptation to other pollutant remediation systems.

4. Conclusions

Illuminated ISW@PDA@NCDs biohybrids obtained an outstanding Cr(VI) reduction performance with a high efficiency (up to 100%) for 100 mg/L Cr(VI) within 72 h, which is 40 times of that of wild strain in

Table 1
Comparison of recent investigations examining Cr(VI) reduction by the *Shewanella* genus.

Species	Incubation biomass	Initial Cr(VI) exposure (mg/L)	Reduction efficiency (mg/(L·h))	Bioreduction effect (%)	Mediating material	Illumination condition	Operating condition	Reference
S. loihica PV-4	Unrecorded	52.0	0.080	≈91.2	Pure strain alone	Dark	Anaerobic	Wang et al., (2017)
S. oneidensis MR-1	1 g/L	52.0	4.2	≈65.0	Goethite-humic acid complex	Dark	Anaerobic	Mohamed et al., (2020)
S. oneidensis MR-1	2 g/L	52.0	3.9	≈75.0	Impregnated Ca-alginate capsule	Dark	Anaerobic	Yu et al., (2020)
S. oneidensis MR-1	OD_{600} ≈ 0.2	10.4	0.87	≈50.0	Hematite NPs	Light	Anaerobic	Cheng et al., (2021)
S. oneidensis MR-1	OD_{600} ≈ 0.1	13.0	1.6	≈100	reduced Graphene Oxide (rGO)+Pd NPs	Dark	Anaerobic	Chen et al., (2020)
S. xiamenensis BC01	OD_{600} ≈ 0.3	50.0	1.4	≈100	Graphene oxide (GO)/ Polyvinyl alcohol (PVA) composites	Dark	Aerobic	Luo et al., (2019)
S. xiamenensis BC01	OD_{600} ≈ 0.3	50.0	0.42	≈100	rGO/PVA film	Dark	Anaerobic	Li et al., (2020)
S. xiamenensis BC01	OD_{600} ≈ 0.3	50.0	0.69	≈100	2-hydroxy-1,4-naphthoquinone/GO/PVA composites	Dark	Anaerobic	Li et al., (2019)
S. oneidensis MR-1	10^8 CFU/mL	20.0	0.12	≈100	Anthraquinone-2,6-disulfonate + $Fe(OH)_3$	Dark	Anaerobic	Liu et al. (2019b)
S. oneidensis MR-1	0.5 g/L	52.0	5.2	≈100	Hematite NPs	Light	Anaerobic	Yu et al., (2022)
S. oneidensis MR-1	OD_{600} ≈ 0.3	100	1.4	≈100	PDA + NCDs	Light	Anaerobic	Present study

Note: according to the relationship between OD_{600} and biomass values (Fig. S2), the biomass with an OD_{600} of 0.3 in this work corresponds to ~0.38 g/L.

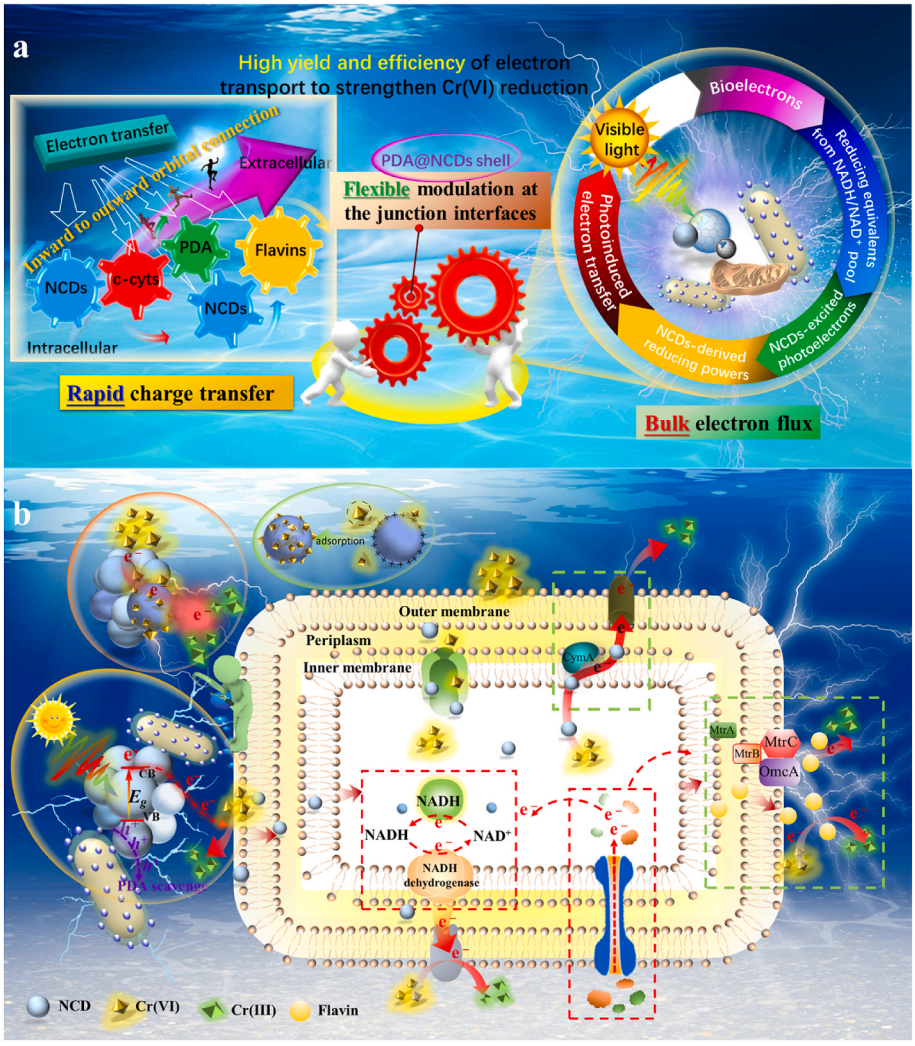

Fig. 7. Schematic of the visible light-enhanced, microbial-photoreductive Cr(VI) process in the presence of illuminated ISW@PDA@NCDs biohybrids based on mechanisms proposed by Martinez and Alvarez, (2018), Li et al., (2019) and Li et al., (2020). In Fig. 7b, the dotted boxes, lines and arrows in red indicate the increased electron flux, and the dotted boxes, lines and arrows in green indicate the process or key interface of rapid charge transfer. (For interpretation of the references to color in this figure legend, the reader is referred to the Web version of this article.)

the dark. Architecture of inward-to-outward modular assemblies of NCDs, PDA and *S. oneidensis* MR-1 supplies more foreign electrons harvested from illuminated NCDs and reducing powers to boost Cr(VI) reduction and simultaneously circumvents low efficient electron transfers at electronic abiotic/biotic interfaces. Meanwhile, the productions of c-cyts, flavins and NADH/NAD^+ pool in ISW@PDA@NCDs cells were more than 6.7, 1.7 and 1.2 times higher than that of wild strain. These improvements will harness more electron-transfer conduits or electron-shuttling orbits to living biohybrids. The improvement ensures an efficient efficiency-configuration framework aiming to promote electron-exporting capability. Our study gives a boost to the Cr(VI)-remediation strategy based on traditional microbial technology.

5. Author contributions statement

Jian Li: Experiment & Writing-original draft. Feng Wang: Experiment & Information Survey. Jing Zhang: Conceptualization, Methodology. Honghui Wang: Information Survey & Collection. Chongyuan Zhao: Methodology & Software. Lielin Shu: Investigation. Peng Huang: Investigation. Yejing Xu: Information Survey. Zhiying Yan: Formal Analysis. Randy A. Dahlgren: Review & Editing. Zheng Chen: Funding Acquisition, Supervision, Review & Editing.

Declaration of competing interest

The authors declare that they have no known competing financial interests or personal relationships that could have appeared to influence the work reported in this paper.

Data availability

The authors do not have permission to share data.

Acknowledgments

This work was supported by the National Natural Science Foundation of China (41807035), Zhejiang Province Public Welfare Technology Application Research Project (LGF22E080002), and the Open Fund of Chengdu Institute of Biology, Chinese Academy of Sciences (KLCAS-2019-4).

Appendix B. Supplementary data

Supplementary data to this article can be found online at https://doi.org/10.1016/j.chemosphere.2022.135980.

Appendix A. Supplementary data

Supplementary material related to this article can be found in the online version.

References

Aggarwal, R., Saini, D., Sonkar, S.K., Sonker, A.K., Westman, G., 2022. Sunlight promoted removal of toxic hexavalent chromium by cellulose derived photoactive carbon dots. Chemosphere 287, 132287.

Anand, S.R., Aggarwal, R., Saini, D., Sonker, A.K., Chauhan, N., Sonkar, S.K., 2019. Removal of toxic chromium (VI) from the wastewater under the sunlight-illumination by functionalized carbon nano-rods. Sol. Energy 193, 774–781.

Apetrei, R.-M., Carac, G., Ramanaviciene, A., Bahrim, G., Tanase, C., Ramanavicius, A., 2019. Cell-assisted synthesis of conducting polymer – polypyrrole – for the improvement of electric charge transfer through fungal cell wall. Colloids Surf., B 175, 671–679.

Bhati, A., Anand, S.R., Saini, D., Gunture Sonkar, S.K., 2019. Sunlight-induced photoreduction of Cr(VI) to Cr(III) in wastewater by nitrogen-phosphorus-doped carbon dots. npj Clean Water 2, 12.

Brutinel, E.D., Gralnick, J.A., 2012. Shuttling happens: soluble flavin mediators of extracellular electron transfer in *Shewanella*. Appl. Microbiol. Biotechnol. 93, 41–48.

Cestellos-Blanco, S., Zhang, H., Kim, J.M., Shen, Y.X., Yang, P.D., 2020. Photosynthetic semiconductor biohybrids for solar-driven biocatalysis. Nature Catalysis 3, 245–255.

Chen, X., Li, S., Liu, L., 2014. Engineering redox balance through cofactor systems. Trends Biotechnol. 32, 337–343.

Chen, Y.-X., Liu, X., Fang, Z., Zhang, C.-L., Abbas, S.Z., Yu, Y.-Y., Yong, Y.-C., 2020. Self-assembling of *Shewanella*@rGO@Pd bionanohybrid for synergistic bio-abiotic removal of Cr(VI). J. Appl. Chem. Biotechnol. 95, 2222–2228.

Chen, Z., Zhang, J., Lyu, Q., Wang, H., Ji, X., Yan, Z., Chen, F., Dahlgren, R.A., Zhang, M., 2022. Modular configurations of living biomaterials incorporating nano-based artificial mediators and synthetic biology to improve bioelectrocatalytic performance: a review. Sci. Total Environ. 824, 153857.

Cheng, H., Jing, Z., Yang, L., Lu, A., Ren, G., Liu, J., 2021. Sunlight-triggered synergy of hematite and *Shewanella oneidensis* MR-1 in Cr(VI) removal. Geochem. Cosmochim. Acta 305, 19–32.

Der, B.S., Machius, M., Miley, M.J., Mills, J.L., Szyperski, T., Kuhlman, B., 2012. Metal-mediated affinity and orientation specificity in a computationally designed protein homodimer. J. Am. Chem. Soc. 134, 375–385.

Dhenadhayalan, N., Lin, K.-C., Saleh, T.A., 2020. Recent advances in functionalized carbon dots toward the design of efficient materials for sensing and catalysis applications. Small 16, 1905767.

Ding, Y., Bertram, J.R., Eckert, C., Bommareddy, R.R., Patel, R., Conradie, A., Bryan, S., Nagpal, P., 2019. Nanorg microbial factories: light-driven renewable biochemical synthesis using quantum dot-bacteria nanobiohybrids. J. Am. Chem. Soc. 141, 10272–10282.

Dong, G., Chen, Y., Yan, Z., Zhang, J., Ji, X., Wang, H., Dahlgren, R.A., Chen, F., Shang, X., Chen, Z., 2020a. Recent advances in the roles of minerals for enhanced microbial extracellular electron transfer. Renew. Sustain. Energy Rev. 134, 110404.

Dong, G., Han, R., Pan, Y., Zhang, C., Liu, Y., Wang, H., Ji, X., Dahlgren, R.A., Shang, X., Chen, Z., Zhang, M., 2021. Role of MnO_2 in controlling iron and arsenic mobilization from illuminated flooded arsenic-enriched soils. J. Hazard Mater. 401, 123362.

Dong, G., Wang, H., Yan, Z., Zhang, J., Ji, X., Lin, M., Dahlgren, R.A., Shang, X., Zhang, M., Chen, Z., 2020b. Cadmium sulfide nanoparticles-assisted intimate coupling of microbial and photoelectrochemical processes: mechanisms and environmental applications. Sci. Total Environ. 740, 140080.

Fang, X., Kalathil, S., Reisner, E., 2020. Semi-biological approaches to solar-to-chemical conversion. Chem. Soc. Rev. 49, 4926–4952.

Guo, D., Wei, H.-F., Song, R.-B., Fu, J., Lu, X., Jelinek, R., Min, Q., Zhang, J.-R., Zhang, Q., Zhu, J.-J., 2019. N,S-doped carbon dots as dual-functional modifiers to boost bio-electricity generation of individually-modified bacterial cells. Nano Energy 63, 103875.

Ha, T.Q., Planje, I.J., White, J.R.G., Aragonès, A.C., Díez-Pérez, I., 2021. Charge transport at the protein–electrode interface in the emerging field of bioMolecular electronics. Curr. Opin. Electroch. 28, 100734.

Han, J.-C., Chen, G.-J., Qin, L.-P., Mu, Y., 2017. Metal respiratory pathway-independent Cr isotope fractionation during Cr(VI) reduction by *Shewanella oneidensis* MR-1. Environ. Sci. Technol. Lett. 4, 500–504.

Heidary, N., Kornienko, N., Kalathil, S., Fang, X., Ly, K.H., Greer, H.F., Reisner, E., 2020. Disparity of cytochrome utilization in anodic and cathodic extracellular electron transfer pathways of *Geobacter sulfurreducens* biofilms. J. Am. Chem. Soc. 142, 5194–5203.

Huang, S., Tang, J., Liu, X., Dong, G., Zhou, S., 2019. Fast light-driven biodecolorization by a *Geobacter sulfurreducens*–CdS biohybrid. ACS Sustain. Chem. Eng. 7, 15427–15433.

Khare, P., Bhati, A., Anand, S.R., Gunture Sonkar, S.K., 2018. Brightly fluorescent zinc-doped red-emitting carbon dots for the sunlight-induced photoreduction of Cr(VI) to Cr(III). ACS Omega 3, 5187–5194.

Khare, P., Yadav, A., Ramkumar, J., Verma, N., 2016. Microchannel-embedded metal–carbon–polymer nanocomposite as a novel support for chitosan for efficient removal of hexavalent chromium from water under dynamic conditions. Chem. Eng. J. 293, 44–54.

Kortemme, T., Morozov, A.V., Baker, D., 2003. An orientation-dependent hydrogen bonding potential improves prediction of specificity and structure for proteins and protein–protein complexes. J. Mol. Biol. 326, 1239–1259.

Li, F., Li, Y.-X., Cao, Y.-X., Wang, L., Liu, C.-G., Shi, L., Song, H., 2018a. Modular engineering to increase intracellular NAD(H/$^+$) promotes rate of extracellular electron transfer of *Shewanella oneidensis*. Nat. Commun. 9, 3637.

Li, F., Li, Y., Sun, L., Chen, X., An, X., Yin, C., Cao, Y., Wu, H., Song, H., 2018b. Modular engineering intracellular NADH regeneration boosts extracellular electron transfer of *Shewanella oneidensis* MR-1. ACS Synth. Biol. 7, 885–895.

Li, F., Wang, L., Liu, C., Wu, D., Song, H., 2018c. Engineering exoelectrogens by synthetic biology strategies. Curr. Opin. Electroch. 10, 37–45.

Li, Y., Chen, Z., Shi, Y., Luo, Q., Wang, Y., Wang, H., Peng, Y., Wang, H., He, N., Wang, Y., 2020. Function of *c*-type cytochromes of *Shewanella xiamenensis* in enhanced anaerobic bioreduction of Cr(VI) by graphene oxide and graphene oxide/polyvinyl alcohol films. J. Hazard Mater. 387, 122018.

Li, Y., Luo, Q., Li, H., Chen, Z., Shen, L., Peng, Y., Wang, H., He, N., Li, Q., Wang, Y., 2019. Application of 2-hydroxy-1, 4-naphthoquinone-graphene oxide (HNQ-GO) composite as recyclable catalyst to enhance Cr(VI) reduction by *Shewanella xiamenensis*. J. Appl. Chem. Biotechnol. 94, 446–454.

Lin, T., Ding, W., Sun, L., Wang, L., Liu, C.-G., Song, H., 2018. Engineered *Shewanella oneidensis*-reduced graphene oxide biohybrid with enhanced biosynthesis and transport of flavins enabled a highest bioelectricity output in microbial fuel cells. Nano Energy 50, 639–648.

Liu, F., Rotaru, A.-E., Shrestha, P.M., Malvankar, N.S., Nevin, K.P., Lovley, D.R., 2015. Magnetite compensates for the lack of a pilin-associated c-type cytochrome in extracellular electron exchange. Environ. Microbiol. 17, 648–655.

Liu, S.-R., Cai, L.-F., Wang, L.-Y., Yi, X.-F., Peng, Y.-J., He, N., Wu, X., Wang, Y.-P., 2019a. Polydopamine coating on individual cells for enhanced extracellular electron transfer. Chem. Commun. 55, 10535–10538.

Liu, S., Yi, X., Wu, X., Li, Q., Wang, Y., 2020. Internalized carbon dots for enhanced extracellular electron transfer in the dark and light. Small 16, 2004194.

Liu, X., Chu, G., Du, Y., Li, J., Si, Y., 2019b. The role of electron shuttle enhances Fe(III)-mediated reduction of Cr(VI) by *Shewanella oneidensis* MR-1. World J. Microbiol. Biotechnol. 35, 64.

Luo, Q., Chen, Z., Li, Y., Wang, Y., Cai, L., Wang, L., Liu, S., Wang, Z., Peng, Y., Wang, Y., 2019. Highly efficient and recyclable *Shewanella xiamenensis*-grafted Graphene Oxide/Poly(vinyl alcohol) biofilm catalysts for increased Cr(VI) reduction. ACS Sustain. Chem. Eng. 7, 12611–12620.

Martinez, C.M., Alvarez, L.H., 2018. Application of redox mediators in bioelectrochemical systems. Biotechnol. Adv. 36, 1412–1423.

Mohamed, A., Yu, L., Fang, Y., Ashry, N., Riahi, Y., Uddin, I., Dai, K., Huang, Q., 2020. Iron mineral-humic acid complex enhanced Cr(VI) reduction by *Shewanella oneidensis* MR-1. Chemosphere 247, 125902.

Mullet, M., Demoisson, F., Humbert, B., Michot, L.J., Vantelon, D., 2007. Aqueous Cr(VI) reduction by pyrite: speciation and characterisation of the solid phases by X-ray photoelectron, Raman and X-ray absorption spectroscopies. Geochem. Cosmochim. Acta 71, 3257–3271.

Nguyen, P.Q., Courchesne, N.-M.D., Duraj-Thatte, A., Praveschotinunt, P., Joshi, N.S., 2018. Engineered living materials: prospects and challenges for using biological systems to direct the assembly of smart materials. Adv. Mater. 30, 1704847.

Park, J.H., Yang, S.H., Lee, J., Ko, E.H., Hong, D., Choi, I.S., 2014. Nanocoating of single cells: from maintenance of cell viability to manipulation of cellular activities. Adv. Mater. 26, 2001–2010.

Richardson, D.J., Butt, J.N., Fredrickson, J.K., Zachara, J.M., Shi, L., Edwards, M.J., White, G., Baiden, N., Gates, A.J., Marritt, S.J., Clarke, T.A., 2012. The 'porin-cytochrome' model for microbe-to-mineral electron transfer. Mol. Microbiol. 85, 201–212.

Saini, D., Kaushik, J., Garg, A.K., Dalal, C., Sonkar, S.K., 2020. N, S-codoped carbon dots for nontoxic cell imaging and as a sunlight-active photocatalytic material for the removal of chromium. ACS Appl. Bio Mater. 3, 3656–3663.

Sakimoto, K.K., Zhang, S.J., Yang, P., 2016. Cysteine–cystine photoregeneration for oxygenic photosynthesis of acetic acid from CO_2 by a tandem inorganic–biological hybrid system. Nano Lett. 16, 5883–5887.

Sivakumar, K., Wang, V.B., Chen, X., Bazan, G.C., Kjelleberg, S., Loo, S.C.J., Cao, B., 2014. Membrane permeabilization underlies the enhancement of extracellular bioactivity in *Shewanella oneidensis* by a membrane-spanning conjugated oligoelectrolyte. Appl. Microbiol. Biotechnol. 98, 9021–9031.

Song, R.-B., Wu, Y., Lin, Z.-Q., Xie, J., Tan, C.H., Loo, J.S.C., Cao, B., Zhang, J.-R., Zhu, J.-J., Zhang, Q., 2017. Living and conducting: coating individual bacterial cells with in situ ormed polypyrrole. Angew. Chem., Int. Ed. 56, 10516–10520.

Svitkova, V., Blaskovicova, J., Tekelova, M., Kallai, B.M., Ignat, T., Horackova, V., Skladal, P., Kopel, P., Adam, V., Farkasova, D., Labuda, J., 2017. Assessment of CdS quantum dots effect on UV damage to DNA using a DNA/quantum dots structured electrochemical biosensor and DNA biosensing in solution. Sens. Actuat. B-chem 243, 435–444.

Sytnyk, M., Jakešová, M., Litviňuková, M., Mashkov, O., Kriegner, D., Stangl, J., Nebesářová, J., Fecher, F.W., Schöfberger, W., Sariciftci, N.S., Schindl, R., Heiss, W., Głowacki, E.D., 2017. Cellular interfaces with hydrogen-bonded organic semiconductor hierarchical nanocrystals. Nat. Commun. 8, 91.

Thirumalaivasan, N., Wu, S.-P., 2020. Bright luminescent carbon dots for multifunctional selective sensing and imaging applications in living cells. ACS Appl. Bio Mater. 3, 6439–6446.

Verma, N.K., Khare, P., Verma, N., 2015. Synthesis of iron-doped resorcinol formaldehyde-based aerogels for the removal of Cr(VI) from water. Green Process. Synth. 4, 37–46.

Wang, G., Zhang, B., Li, S., Yang, M., Yin, C., 2017. Simultaneous microbial reduction of vanadium (V) and chromium (VI) by *Shewanella loihica* PV-4. Bioresour. Technol. 227, 353–358.

Yang, C., Aslan, H., Zhang, P., Zhu, S., Xiao, Y., Chen, L., Khan, N., Boesen, T., Wang, Y., Liu, Y., Wang, L., Sun, Y., Feng, Y., Besenbacher, F., Zhao, F., Yu, M., 2020. Carbon dots-fed *Shewanella oneidensis* MR-1 for bioelectricity enhancement. Nat. Commun. 11, 1379.

Yong, X.-Y., Feng, J., Chen, Y.-L., Shi, D.-Y., Xu, Y.-S., Zhou, J., Wang, S.-Y., Xu, L., Yong, Y.-C., Sun, Y.-M., Shi, C.-L., OuYang, P.-K., Zheng, T., 2014. Enhancement of

bioelectricity generation by cofactor manipulation in microbial fuel cell. Biosens. Bioelectron. 56, 19–25.
Yu, C., Yu, L., Mohamed, A., Fang, J., Wu, Y., Dai, K., Cai, P., Huang, Q., 2022. Size-dependent visible-light-enhanced Cr(VI) bioreduction by hematite nanoparticles. Chemosphere 295, 133633.
Yu, C., Zhang, Y., Fang, Y., Tan, Y., Dai, K., Liu, S., Huang, Q., 2020. *Shewanella oneidensis* MR-1 impregnated Ca-alginate capsule for efficient Cr(VI) reduction and Cr(III) adsorption. Environ. Sci. Pollut. Res. 27, 16745–16753.